Air-stable and visible-light-active p-type organic long-persistent-luminescence system by using organic photoredox catalyst

Kazuya Jinnai
Center for Organic Photonics and Electronics Research (OPERA), Kyushu University
https://orcid.org/0000-0002-1153-0205
Ryota Kabe
Okinawa Institute of Science and Technology Graduate University https://orcid.org/0000-0002-3647-4262
Zesen Lin
Organic Optoelectronics Unit, Okinawa Institute of Science and Technology Graduate University
Chihaya Adachi (adachi@cstf.kyushu-u.ac.jp)
Kyushu University https://orcid.org/0000-0001-6117-9604

Article

Keywords: organic photoredox catalyst, Organic long-persistent-luminescent (OLPL) materials, inorganic materials

Posted Date: February 19th, 2021

DOI: https://doi.org/10.21203/rs.3.rs-248708/v1

Version of Record: A version of this preprint was published at Nature Materials on November 29th, 2021.
See the published version at https://doi.org/10.1038/s41563-021-01150-9.

Abstract

Organic long-persistent-luminescent (OLPL) materials that exhibit hour-long photoluminescence have advantages over inorganic materials, such as a sustainability, flexibility, and processability. The OLPL materials store the absorbed energy in an intermediate charge-separated state, but this charge-separated state is unstable to oxygen and does not exhibit persistent luminescence in air. The excitation wavelength of OLPL can be controlled by electron-donor and -acceptor materials, but previous materials require absorption mainly in the ultraviolet region.

Here, we show OLPL systems that exhibit a persistent luminescence in air and can be excited by a wavelength from 300-nm to 600-nm. By using cationic photoredox catalysts as an electron-accepting dopant, stable charge-separated states are generated by the hole-diffusion process, as opposed to previous OLPL systems that depend on electron diffusion. By using a hole-diffusion mechanism and reducing the energy level of the lowest unoccupied molecular orbital, the OLPL system becomes stable in air and can be excited by visible light. The addition of hole-trapping material increases the LPL duration.

1. Introduction

Long-persistent luminescence (LPL) is a phenomenon in which luminescence persists for a long period after photoexcitation[1]. LPL emitters are used as glow-in-the-dark paints for clock faces and emergency lights. High-efficiency LPL materials are composed of metal-oxide microcrystals and small amounts of rare-earth ions that act as charge-trapping and emission sites[2,3]. In these inorganic LPL materials, holes or electrons generated by the photoexcitation of the metal-oxide-crystal are accumulated in dopants that act as charge trap sites. Gradual charge recombination followed by thermal detrapping produces hour-long emissions[4–6]. Inorganic LPL materials are insoluble in any solvent that requires extra processes for applications. Most inorganic LPL systems require ultraviolet (UV) to blue excitation light below 450-nm because of the limited metal-oxide absorption bands[7–9].

We have reported LPL emissions from mixtures of organic molecules[10]. This organic LPL (OLPL) system can be fabricated from a solution process[11] and the fabricated films can be transparent and flexible[12]. The LPL emission can be tuned from greenish-blue to red by fluorescent material addition[13]. In contrast to conventional organic room-temperature phosphorescent (RTP) materials[14], which store their energy in triplet excited states and exhibit radiative transition from the triplet excited states to the singlet ground states[15], OLPL systems accumulate energy into charge-separated states similar to inorganic LPL materials. LPL and RTP can be identified from their emission decay profiles[16–18].

Current OLPL systems require inert gas conditions to exhibit LPL because LPL is quenched completely in air. The OLPL system, which is comprised of an electron-donating and an electron-accepting material, stores absorbed energy into geminate pairs of the air-unstable donor radical cations and the acceptor radical anions. A donor–acceptor mixed crystal reported by Tang et al. exhibits OLPL in air because oxygen diffusion is suppressed by crystallization[19]. However, the crystalline system cannot take

advantage of the OLPL material properties, such as their flexibility and processability. For practical applications of OLPL systems, the air-stability needs to be improved without crystallization.

Organic field-effect transistors use radical cations and anions as the active charge-transport species, but many air-stable organic transistors have been reported[20]. Radical anions (n-type organic semiconductors) are more unstable than radical cations (p-type organic semiconductors) in air. The reported OLPL systems can be considered as an n-type OLPL system because the donor concentration is low and only electrons can diffuse through acceptor molecules (Fig. 1a). The unstable radical anions can be ascribed to the high probability of reaction with oxygen. A p-type OLPL system, in which radical cations diffuse (Fig. 1a), is expected to be more stable to oxygen. Air-stable organic transistors have been achieved by making the lowest unoccupied molecular orbital (LUMO) level deeper than the reduction potential of oxygen (–3.5 eV) [21,22]. To improve the air stability of the OLPL systems, the p-type OLPL system with deep highest occupied molecular orbital (HOMO) and LUMO levels is required.

To satisfy these requirements, we focused on cationic electron acceptors, which are termed organic photoredox catalysts[23]. The organic photoredox catalysts are ideal electron acceptors because of their high oxidation potential in the excited state and their ability to form a stable one-electron reduced state. Many organic photoredox catalysts have a large enough energy gap to exhibit luminescence in the visible region. Furthermore, a mixture of neutral donors and acceptors forms radical ion pairs (D^{d+}–A^{d-}) with Coulomb interaction by photo-induced charge separation, whereas cationic acceptors or anionic donors form neutral radicals rather than radical anions or cations (D^{d+}– $(A^{+})^{d-}$, $(D^{-})^{d+}$–A^{d-}) (Fig. 1b). Even if there are counter ions, the formation of neutral radicals is expected to reduce the Coulomb interaction in the charge-separated state[19,24,25].

Further stabilization of the charge-separated states is required even though the Coulomb interaction is reduced. Similar to inorganic LPL systems, the charge-separated state is expected to be stabilized by a special separation of the ion pairs by the introduction of carrier trap materials[26,27].

Here, we report air-stable p-type OLPL systems made from cationic electron acceptors as a dopant and neutral electron donors as a host. These systems exhibit sufficient LPL performance in air. The addition of hole-trap materials improved the performance sixfold under nitrogen gas without changing the emission spectrum. In addition to the air stability, the p-type OLPL system can be excited by a wavelength from 300-nm to 600-nm. By tuning the energy gap between the electron donor and acceptor, near-infrared (NIR) LPL emission is achieved. The development of such air-stable and visible-light-active p-type OLPL systems will contribute to various future practical applications of OLPL systems.

2. Results And Discussion

Cationic photoredox catalysts, 2,4,6-triphenylpyrylium tetrafluoroborate (TPP^{+}) and 2,4,6-tris(methoxyphenyl)pyrylium tetrafluoroborate ($MeOTPP^{+}$) were used as electron acceptors[28–30] and semiconducting host molecules 3,3'-di(9*H*-carbazol-9-yl)biphenyl (*m*CBP)[31] and 1,3,5-tris(1-phenyl-1*H*-

benzimidazol-2-yl)benzene (TPBi)[32] were used as electron donors (Fig. 1c). 4,4',4"-Tri(9-carbazoyl)triphenylamine (TCTA)[33] was used as a hole-trap material. Analytical results of these materials by UV–visible absorption, fluorescence, and phosphorescence spectra are shown in Figure S1. Energy levels of the lowest singlet excited state (^{1}LE) and triplet excited states (^{3}LE) were estimated from the onset of fluorescence and the phosphorescence spectra, respectively. LUMO levels were obtained from the first reduction peaks of the cyclic voltammograms (CV) (Figure S2), and the HOMO levels were estimated from the optical gap that was calculated from the absorption edge (Fig. 1d, Table S1). The HOMO level of the TCTA was obtained from the CV, and the LUMO level was estimated from the optical energy gap because of the electric window of the solvent.

LPL films with a 1:99 molar ratio of acceptor:donor system were fabricated by conventional melt casting[11]. Steady-state photoluminescence (PL) and LPL spectra, emission decay profiles, and PL quantum yields (F_{PL}) were obtained under nitrogen gas. The LPL duration was defined as the time until the emission intensity dropped below 1 pW after 60 s of excitation. The triplet charge-transfer excited state (^{3}CT) level was assumed from the singlet charge-transfer excited state (^{1}CT) level that was obtained from the onset of the PL spectrum because most LPL systems have a small energy gap between the ^{1}CT and ^{3}CT[34].

When the films were excited by 365-nm light, which can only be absorbed by the acceptors, the TPP^+/TPBi, TPP^+/*m*CBP, and $MeOTPP^+$/*m*CBP films exhibited a long LPL emission in which the decay profiles followed a power-law decay (Fig. 2a)[35,36]. This power-law emission decay indicates the generation of intermediate charge-separated states and successive gradual charge recombination, which led to LPL. The emission spectra of these films was attributed to the CT excited states between the donors and acceptors[16,17].

The TPP^+/TPBi, TPP^+/*m*CBP, and $MeOTPP^+$/*m*CBP films form ^{1}CT excited states (Fig. 2b) and the ^{1}CT energy levels are lower than those of the locally excited states of the donors and acceptors (^3LE_D and ^3LE_A). Therefore, the LPL that was caused by the recombination of accumulated charges occurs from the CT states. The TPP^+/TPBi film exhibits a CT emission at 603-nm with a shoulder peak at ~ 555-nm. The shoulder peak decreased with an increase in TPP^+ concentration because of the self-absorption of TPP radicals at 500–600 nm (Figure S3a)[17,37,38] and it disappeared at the higher TPP^+ concentration because of a strong self-absorption of the TPP radical (Figure S3b). The TPP^+/TPBi film showed the longest LPL duration of 1435 s because of the highest F_{PL} of 10.2%. The LPL duration decreased with an increase in TPP^+ concentration because the charge recombination probability increased at the higher TPP^+ concentration (Figure S3c).

The TPP^+/*m*CBP film exhibited a broad NIR emission at 731-nm because of the smaller energy gap between the TPP^+ LUMO and *m*CBP HOMO. Because of the low F_{PL} of the CT emission and low NIR sensitivity of the photodiode for detection, the LPL duration was 19 s. The $MeOTPP^+$/*m*CBP films

exhibited a CT emission at 624-nm with an LPL duration of 605 s. In contrast, the $MeOTPP^+$/TPBi film did not form a CT excited state although the HOMO and LUMO levels were appropriate. The TPBi may not act as a donor because of the closed HOMO levels between them. Instead, this film exhibited the fluorescence and RTP of the $MeOTPP^+$ (Figure S4c). These results indicate that the formation of the lowest ^{1}CT state is important for efficient LPL emission in p-type OLPL systems.

Because a blend film of donor and acceptor molecules has donor, acceptor, and charge-transfer absorption bands, OLPL systems can be excited by various wavelengths, and is a major advantage over inorganic LPL systems, which are limited mostly to UV to blue excitation wavelengths. The excitation spectra of the TPP^+/TPBi and $MeOTPP^+$/*m*CBP films indicate that these films can be excited by a wavelength from 300-nm to 600-nm (Figure S5). To confirm the excitation wavelength dependence of the LPL emission, these films were excited by 365-nm, 400-nm, 455-nm, 500-nm, 550-nm, and 600-nm LEDs. The LPL emission was observed at all excitation wavelengths, although the LPL duration decreased, which correlates with the absorption intensity (Figs. 2c and S5c). The 600-nm photoexcitation and NIR LPL emission, which corresponds to the biological window, is expected to be used for bio-imaging[39].

The LPL performance improved sixfold with hole-trapping material addition to the p-type OLPL system. Previously, we reported that the LPL duration could be enhanced by doping electron-trapping materials into an n-type OLPL system[13]. The dopants can receive electrons from the acceptor molecules because the LUMO of the dopant is lower than that of the acceptor. By tuning the appropriate LUMO level, the trapped electrons remained for more than one week[40]. In the p-type OLPL system, TCTA was doped into the TPP^+/TPBi system because the HOMO level of the TCTA (−5.3 eV) was shallower than that of the TPBi (−5.9 eV) (Fig. 1d and Figure S2). The PL and LPL spectra of the TPP^+/TPBi/TCTA film with a 1:99:1 molar ratio were identical to that of the TPP^+/TPBi film (Fig. 3a) but the LPL duration improved sixfold to 9045 s (Fig. 3b). This result indicates that the TCTA acts as hole traps to the charge-separated state (Fig. 3c, Figure S6a).

To confirm the hole trapping by TCTA, absorption spectra of the TPP^+/TPBi and TPP^+/TPBi/TCTA films were obtained[40]. After photoexcitation, a clear broad absorption above 800-nm was observed in the TPP^+/TPBi/TCTA film (Fig. 3d). This peak corresponds to the radical cation of TCTA in dichloromethane (DCM) under electrical oxidation, although a wavelength shift can be observed because of the polarization effect in the solid film (Fig. 3d). The hole trapping was confirmed by the temperature dependence of the LPL duration[41]. Because hole detrapping was endothermic, the LPL intensity increased by increasing the temperature in the TPP^+/TPBi/TCTA film (Figure S6b). In contrast, the LPL duration of the TPP^+/TPBi film decreased gradually with an increase in temperature because the nonradiative process was enhanced at a high temperature (Figure S6c). Thus, detrapping in the TPP^+/TPBi/TCTA film for the LPL intensity overwhelmed the nonradiative process at the measured temperatures.

Optical analysis of the TPP^+/TPBi, $MeOTPP^+$/*m*CBP, and TPP^+/TPBi/TCTA films was carried out in the air to confirm the air stability of the p-type OLPL systems because the LUMO levels of the TPP^+ (−4.0 eV) and $MeOTPP^+$ (−3.8 eV) are lower than the reduction potential of oxygen (−3.5 eV). Although the reported n-type OLPL system of the *m*-MTDATA/PPT did not show LPL emissions in air (Figure S7a), all p-type OLPL films exhibited LPL in air (Fig. 4a, b, Figure S7b). The observed LPL durations of all films in air were shorter than in nitrogen. Although the reaction between acceptor radicals and oxygen can be prevented by deeper acceptors' LUMO levels[22], energy transfer from the triplet excited state of the emitters to the molecular oxygen with a triplet ground state (triplet quenching) cannot be prevented[42]. The charge recombination in LPL emissions generates ^{1}CT and ^{3}CT excited states[43], and the ^{3}CT excited states are quenched by oxygen. In contrast, the emission spectra did not change because of no ^{3}LE contribution (Fig. 4c, d). The LPL duration of the TPP^+/TPBi/TCTA in air was extended to 1421 s, which is almost the same as the TPP^+/TPBi film in nitrogen although the F_{PL} of both films is almost identical (Supplementary Video 1). These results indicate that the p-type OLPL system with deep HOMO levels can emit LPL in air but cannot prevent triple quenching by oxygen. Future developments of the CT excited state with a rapid reverse intersystem crossing (RISC) that is faster than the energy transfer to oxygen or advanced encapsulation techniques to prevent oxygen are required to obtain efficient LPL emissions in air.

3. Conclusions

We demonstrated p-type OLPL systems based on the cationic organic photoredox catalyst TPP+ and MeOTPP+ as acceptors. These systems can be excited by a wavelength from the UV range to 600-nm and exhibited a yellow-to-NIR LPL emission. The p-type OLPL with deeper HOMO and LUMO levels can prevent reaction with oxygen and exhibited LPL in air. The hole-trapping dopant enhanced the LPL duration strongly without changing the emission spectrum. The tunable absorption wavelength from 300-nm to 600-nm of OLPL systems provides a major advantage over inorganic materials, and the absorptions and emissions that were fitted to the biological window are expected to have future bio-imaging applications. The p-type OLPLs can prevent reaction with oxygen in the excited state, which makes it possible to produce LPL films by a simple solution. However, because triplet quenching by oxygen cannot be prevented, a rapid RISC system or combination with oxygen barrier materials is required for future practical applications.

Experimental Section

Materials

TPP^+, $MeOTPP^+$, and *m*-MTDATA were from MERCK (Darmstadt, Germany). TPBi and *m*CBP were from TCI Chemical (Tokyo, Japan). PPT was synthesized according to literature[44].

Film fabrication

In a nitrogen-filled glovebox, mixtures of electron donors and acceptors were placed on a template glass substrate with a 100-mm^2 surface area, 0.5-mm depth, and heated to 280 °C for 10 s. After melting, the substrate was cooled rapidly to room temperature.

Optical and electrical measurements

A dichloromethane solution of each material (10^{-5} M) was used to measure absorption, fluorescence, phosphorescence, and absolute photoluminescence quantum yields (F_{PL}). The absorption spectra were measured using a UV–vis–NIR spectrophotometer (LAMBDA 950, Perkin Elmer). The photoluminescence spectra at room temperature and the phosphorescence spectra at 77 K were measured using spectrofluorometers (FP-8600, JASCO, and PMA-12, Hamamatsu Photonics). The Φ_{PL} were measured using an integrating sphere with a photoluminescence measurement unit (Quantaurus-QY, C11347-01, Hamamatsu Photonics). The phosphorescence lifetime of TPP^+ and $MeOTPP^+$ was obtained by time-resolved emission spectra at 77 K measured by spectrometers (PMA-12, Hamamatsu Photonics). Cyclic voltammetry was carried out using an electrochemical analyser (Model 608D + DPV, BAS). Measurements were performed in dried and oxygen-free DMF using 0.1 M tetrabutylammonium hexafluorophosphate as a supporting electrolyte. A platinum wire was used as a counter electrode, with glassy carbon as a working electrode, and Ag/Ag^+ as a reference electrode. Redox potentials were referenced against ferrocene/ferrocenium (Fc/Fc^+). Corresponding LUMO energies of TPP^+, $MeOTPP^+$, TPBi, and *m*CBP and the HOMO energy of the TCTA were calculated from first reduction or oxidation peaks using an absolute value of − 4.8 eV to vacuum for the Fc/Fc^+ redox potential[45]. The absorption spectra of the TPP^+ and TCTA radical species were measured by the *in situ* UV–vis–NIR spectroelectrochemical technique. The UV-vis-NIR spectrophotometer is UV-3600 Plus, SHIMADZU. The TPP^+ radicals and TCTA radical cations were generated by electrical oxidation on the platinum mesh electrode surface in a DCM solution that contained 0.1 M $TBAPF_6$ (BAE, 013510 SEC-C, Thin layer quartz glass spectroelectrochemical cell kit) through the use of an electrochemical analyzer (BAS, Model 610E). The absorption spectra of TCTA radical cations were obtained 30 s after photoexcitation by a 365-nm LED light.

LPL measurements

The LPL spectra and decay profiles were obtained using a measurement system in a glove box[13]. The fabricated films were placed in a dark box and excited by various LEDs wavelengths with bandpass filters (Thorlabs, band width ± 5 nm), an excitation power of 1 $mWcm^{-2}$, and an excitation duration of 60 s. The PL and LPL spectra were recorded using a multichannel spectrometer (PMA-12, C14631-01, Hamamatsu Photonics). Emission decay profiles were obtained without wavelength sensitivity calibration using a silicon photomultiplier (MPPC module, C13366-1350GA, Hamamatsu Photonics). The temperature dependence and the air stability were measured in a cryostat (PS-HT-200, Nagase Techno-Engineering) connected to a turbo molecular pump (HiPace, Pfeiffer Vacuum) and excited using a 365-nm LED (M340L4, Thorlabs) with a bandpass filter (365 nm ± 5 nm) for 60 s. The LPL properties were measured

under vacuum. Samples were kept under air in the dark for 1 week and the optical properties were measured in air.

Declarations

Acknowledgements

This work was supported by the Japan Science and Technology Agency (JST), ERATO, Adachi Molecular Exciton Engineering Project, under JST ERATO Grant Number JPMJER1305, Japan; the International Institute for Carbon Neutral Energy Research (WPI-I^{2}CNER) sponsored by the Ministry of Education, Culture, Sports, Science, and Technology (MEXT), JSPS KAKENHI Grant Numbers JP18H02049 and JP18H04522; and the Kyushu University Platform of Inter/Transdisciplinary Energy Research, young researcher/doctor student support program. We thank K. Kusuhara and N. Nakamura for their assistance with the preparation of TPBi, *m*CBP, and TCTA.

Data availability

The data that support the findings of this study are available within this article and its Supplementary Information, or from the corresponding author upon reasonable request.

Author contributions

K.J. and R.K designed this project. K.J. carried out all experiments. K.J and Z.L. performed the *in situ* spectroelectrochemical measurements. K.J. and R.K. analysed all data. R.K and C.A. supervised the project. All authors contributed to writing the paper and critically commented on the project.

Competing interests

The authors declare no competing interests.

References

1. Xu, J. & Tanabe, S. Persistent luminescence instead of phosphorescence: History, mechanism, and perspective. *J. Lumin.* **205**, 581–620 (2019).
2. Li, Y., Gecevicius, M. & Qiu, J. Long persistent phosphors—from fundamentals to applications. *Chem. Soc. Rev.* **45**, 2090–2136 (2016).
3. Ueda, J., Miyano, S. & Tanabe, S. Formation of Deep Electron Traps by Yb^{3+} Codoping Leads to Super-Long Persistent Luminescence in Ce^{3+} -Doped Yttrium Aluminum Gallium Garnet Phosphors. *ACS Appl. Mater. Interfaces* **10**, 20652–20660 (2018).

4. Majewska, N. *et al.* Study of persistent luminescence and thermoluminescence in $SrSi_2N_2O_2$:Eu^{2+} ,M^{3+} (M = Ce, Dy, and Nd). *Phys. Chem. Chem. Phys.* **22**, 17152–17159 (2020).
5. Vitola, V., Millers, D., Bite, I., Smits, K. & Spustaka, A. Recent progress in understanding the persistent luminescence in $SrAl_2O_4$:Eu,Dy. *Mater. Sci. Technol.* **35**, 1661–1677 (2019).
6. Dorenbos, P. Mechanism of persistent luminescence in $Sr_2MgSi_2O_7$:Eu^{2+}; Dy^{3+}. *Phys. status solidi* **242**, R7–R9 (2005).
7. Li, Y. *et al.* Long persistent and photo-stimulated luminescence in Cr^{3+}-doped Zn–Ga–Sn–O phosphors for deep and reproducible tissue imaging. *J. Mater. Chem. C* **2**, 2657 (2014).
8. Zhuang, Y., Ueda, J., Tanabe, S. & Dorenbos, P. Band-gap variation and a self-redox effect induced by compositional deviation in $ZnxGa_2O_{3+x}$:Cr^{3+} persistent phosphors. *J. Mater. Chem. C* **2**, 5502 (2014).
9. Wu, S., Pan, Z., Chen, R. & Liu, X. *Long Afterglow Phosphorescent Materials* (Springer 2017).
10. Kabe, R. & Adachi, C. Organic long persistent luminescence. *Nature* **550**, 384–387 (2017).
11. Jinnai, K., Nishimura, N., Kabe, R. & Adachi, C. Fabrication-method Independence of Organic Long-persistent Luminescence Performance. *Chem. Lett.* **48**, 270–273 (2019).
12. Lin, Z., Kabe, R., Nishimura, N., Jinnai, K. & Adachi, C. Organic Long-Persistent Luminescence from a Flexible and Transparent Doped Polymer. *Adv. Mater.* **30**, 1803713 (2018).
13. Jinnai, K., Kabe, R. & Adachi, C. Wide-Range Tuning and Enhancement of Organic Long-Persistent Luminescence Using Emitter Dopants. *Adv. Mater.* **30**, (2018).
14. Hirata, S. Recent Advances in Materials with Room-Temperature Phosphorescence: Photophysics for Triplet Exciton Stabilization. *Adv. Opt. Mater.* **5**, 1700116 (2017).
15. Notsuka, N., Kabe, R., Goushi, K. & Adachi, C. Confinement of Long-Lived Triplet Excitons in Organic Semiconducting Host-Guest Systems. *Adv. Funct. Mater.* **27**, 1703902 (2017).
16. Nishimura, N., Lin, Z., Jinnai, K., Kabe, R. & Adachi, C. Many Exciplex Systems Exhibit Organic Long-Persistent Luminescence. *Adv. Funct. Mater.* **30**, 2000795 (2020).
17. Lin, Z., Kabe, R., Wang, K. & Adachi, C. Influence of energy gap between charge-transfer and locally excited states on organic long persistence luminescence. *Nat. Commun.* **11**, 191 (2020).
18. Bhattacharjee, I. & Hirata, S. Highly Efficient Persistent Room-Temperature Phosphorescence from Heavy Atom-Free Molecules Triggered by Hidden Long Phosphorescent Antenna. *Adv. Mater.* **32**, 2001348 (2020).
19. Alam, P. *et al.* Two Are Better Than One: A Design Principle for Ultralong-Persistent Luminescence of Pure Organics. *Adv. Mater.* **32**, 2001026 (2020).
20. Usta, H. *et al.* Design, synthesis, and characterization of ladder-type molecules and polymers. air-stable, solution-processable n-channel and ambipolar semiconductors for thin-film transistors via experiment and theory. *J. Am. Chem. Soc.* **131**, 5586–5608 (2009).
21. de Leeuw, D. M., Simenon, M. M. J., Brown, A. R. & Einerhand, R. E. F. Stability of n-type doped conducting polymers and consequences for polymeric microelectronic devices. *Synth. Met.* **87**, 53–

59 (1997).

22. Zhou, K., Dong, H., Zhang, H. & Hu, W. High performance n-type and ambipolar small organic semiconductors for organic thin film transistors. *Phys. Chem. Chem. Phys.* **16**, 22448–22457 (2014).
23. Romero, N. A. & Nicewicz, D. A. Organic Photoredox Catalysis. *Chem. Rev.* **116**, 10075–10166 (2016).
24. Fukuzumi, S. *et al.* Electron-transfer state of 9-mesityl-10-methylacridinium ion with a much longer lifetime and higher energy than that of the natural photosynthetic reaction center. *J. Am. Chem. Soc.* **126**, 1600–1601 (2004).
25. Todd, W. P., Dinnocenzo, J. P., Farid, S., Goodman, J. L. & Gould, I. R. Efficient photoinduced generation of radical cations in solvents of medium and low polarity. *J. Am. Chem. Soc.* **113**, 3601–3602 (1991).
26. Jia, D. Charging curves and excitation spectrum of long persistent phosphor $SrAl_2O_4$:Eu^{2+}, Dy^{3+}. *Opt. Mater. (Amst).* **22**, 65–69 (2003).
27. Jia, D., Zhu, J. & Wu, B. Correction of excitation spectra of long persistent phosphors. *J. Lumin.* **90**, 33–37 (2000).
28. Wintgens, V., Pouliquen, J., Kossanyi, J., Williams, J. L. R. & Doty, J. C. Emission of substituted pyrylium and thiapyrylium salts: Phosphorescence and delayed fluorescence emission in polymeric matrices. *Polym. Photochem.* **6**, 1–20 (1985).
29. Farid, S., Dinnocenzo, J. P., Merkel, P. B., Young, R. H. & Shukla, D. Bimolecular Electron Transfers That Follow a Sandros–Boltzmann Dependence on Free Energy. *J. Am. Chem. Soc.* **133**, 4791–4801 (2011).
30. Perkowski, A. J., You, W. & Nicewicz, D. A. Visible Light Photoinitiated Metal-Free Living Cationic Polymerization of 4-Methoxystyrene. *J. Am. Chem. Soc.* **137**, 7580–7583 (2015).
31. Schrögel, P. *et al.* Meta-linked CBP-derivatives as host materials for a blue iridium carbene complex. *Org. Electron.* **12**, 2047–2055 (2011).
32. Jiang, Z.-L., Tian, W., Kou, Z.-Q., Cheng, S. & Li, Y.-H. The influence of the mixed host emitting layer based on the TCTA and TPBi in blue phosphorescent OLED. *Opt. Commun.* **372**, 49–52 (2016).
33. Kuwabara, Y., Ogawa, H., Inada, H., Noma, N. & Shirota, Y. Thermally stable multilared organic electroluminescent devices using novel starburst molecules, 4,4',4"-Tri(N-carbazolyl)triphenylamine (TCTA) and 4,4',4"-Tris(3-methylphenylphenylamino)triphenylamine (*m*-MTDATA), as hole-transport materials. *Adv. Mater.* **6**, 677–679 (1994).
34. Goushi, K., Yoshida, K., Sato, K. & Adachi, C. Organic light-emitting diodes employing efficient reverse intersystem crossing for triplet-to-singlet state conversion. *Nat. Photonics* **6**, 253–258 (2012).
35. Hamill, W. H. Debye–Edwards electron recombination kinetics. *J. Chem. Phys.* **71**, 140–142 (1979).
36. Tachiya, M. & Seki, K. Unified explanation of the fluorescence decay and blinking characteristics of semiconductor nanocrystals. *Appl. Phys. Lett.* **94**, 081104 (2009).
37. Niizuma, S. *et al.* Free Radicals Produced from the Derivatives of Pyrylium Salts in Solution by Photoillumination. *Bull. Chem. Soc. Jpn.* **58**, 2600–2607 (1985).

38. Miranda, M. A. & García, H. 2,4,6-Triphenylpyrylium Tetrafluoroborate as an Electron-Transfer Photosensitizer. *Chem. Rev.* **94**, 1063–1089 (1994).
39. Lochner, C. M., Khan, Y., Pierre, A. & Arias, A. C. All-organic optoelectronic sensor for pulse oximetry. *Nat. Commun.* **5**, 5745 (2014).
40. Sakurai, M. *et al.* Organic Photostimulated Luminescence Organic photostimulated luminescence. 1–32 (2020) doi:org/10.26434/chemrxiv.12956456.v1.
41. Ueda, J., Harada, M., Miyano, S., Yamada, A. & Tanabe, S. Pressure-induced variation of persistent luminescence characteristics in $Y_3Al_{5-x}Ga_xO_{12}:Ce^{3+}–M^{3+}$ (M = Yb, and Cr) phosphors: opposite trend of trap depth for 4f and 3d metal ions. *Phys. Chem. Chem. Phys.* **22**, 19502–19511 (2020).
42. Hasebe, N. *et al.* Absolute Phosphorescence Quantum Yields of Singlet Molecular Oxygen in Solution Determined Using an Integrating Sphere Instrument. *Anal. Chem.* **87**, 2360–2366 (2015).
43. Baldo, M. A., O'Brien, D. F., Thompson, M. E. & Forrest, S. R. Excitonic singlet-triplet ratio in a semiconducting organic thin film. *Phys. Rev. B* **60**, 14422–14428 (1999).
44. Fan, C. *et al.* Dibenzothiophene-Based Phosphine Oxide Host and Electron-Transporting Materials for Efficient Blue Thermally Activated Delayed Fluorescence Diodes through Compatibility Optimization. *Chem. Mater.* **27**, 5131–5140 (2015).
45. Liu, Y., Liu, M. S. & Jen, A. K.-Y. Synthesis and characterization of a novel and highly efficient light-emitting polymer. *Acta Polym.* **50**, 105–108 (1999).

Figures

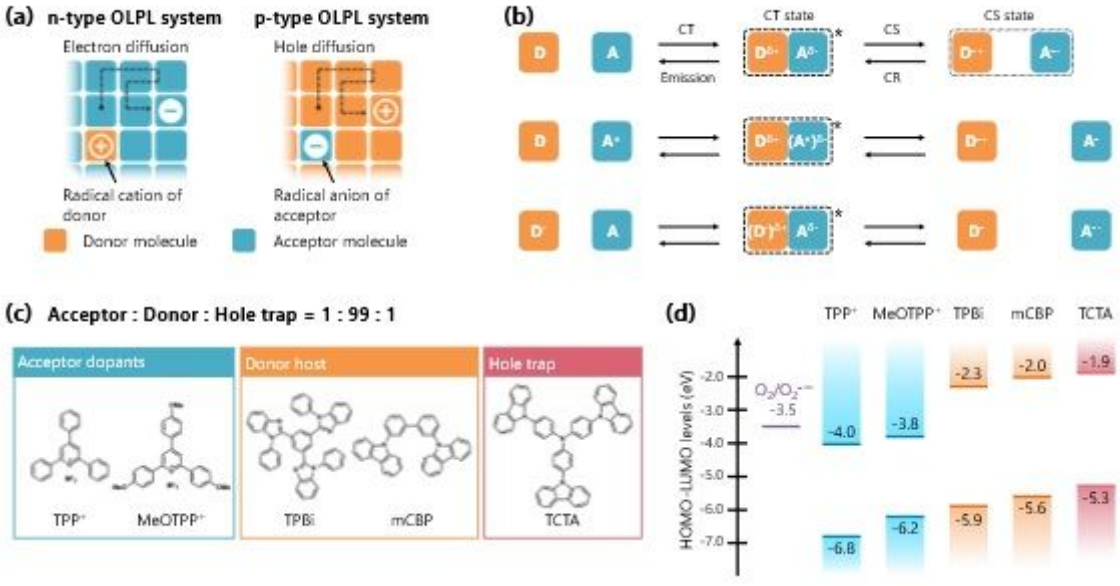

Figure 1

Emission mechanism of p-type OLPL system. (a) Schematic diagram of charge-separated states of n- and p-type OLPL systems. Radical anions of acceptor diffusion in n-type OLPL system and radical cations of donor diffusion in p-type system. (b) Charge-separated states of neutral and ionized molecules. Cationic acceptor and anionic donor can form neutral radicals. (c) Chemical structures of electron acceptors, donors, and hole-trap molecule. (d) HOMO and LUMO levels of materials and oxygen reduction potential.

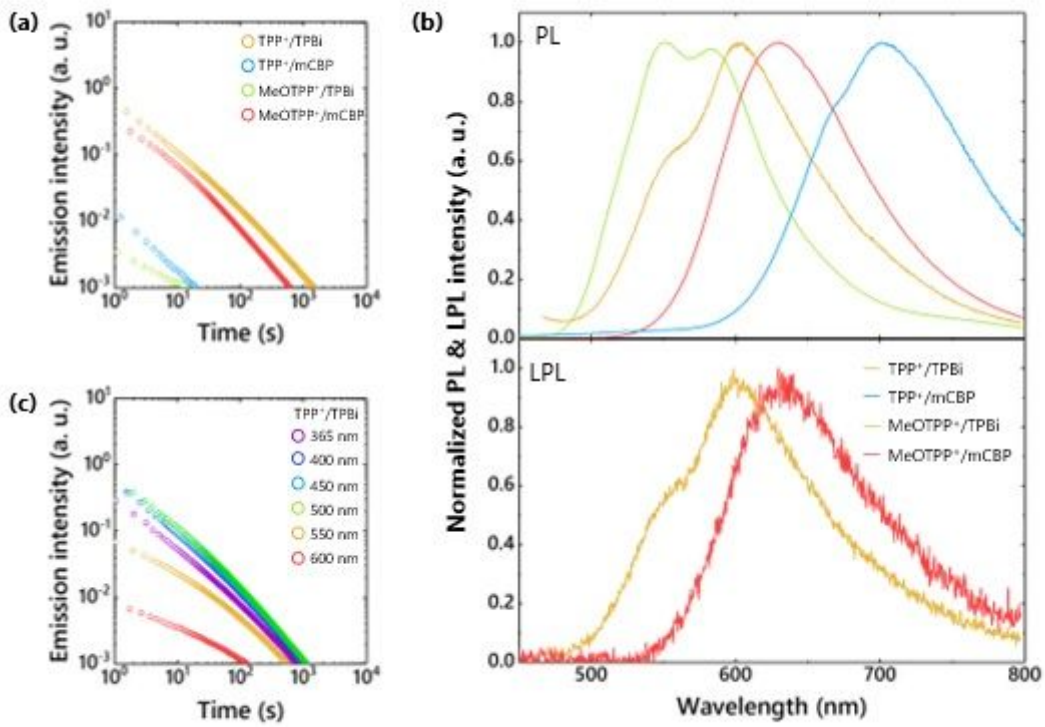

Figure 2

Photoluminescence properties of OLPL systems under nitrogen gas. (a) Emission decay profiles of TPP+/TPBi, TPP+/mCBP, MeOTPP+/TPBi, and MeOTPP+/mCBP films in log–log plot. (b) Steady-state photoluminescence (PL) spectra and emission spectra 10 s after photoexcitation (LPL). The LPL spectrum of the TPP+/mCBP was not measurable because of the weak emission intensity. (c) Excitation-wavelength dependence of emission decay profiles of TPP+/TPBi film.

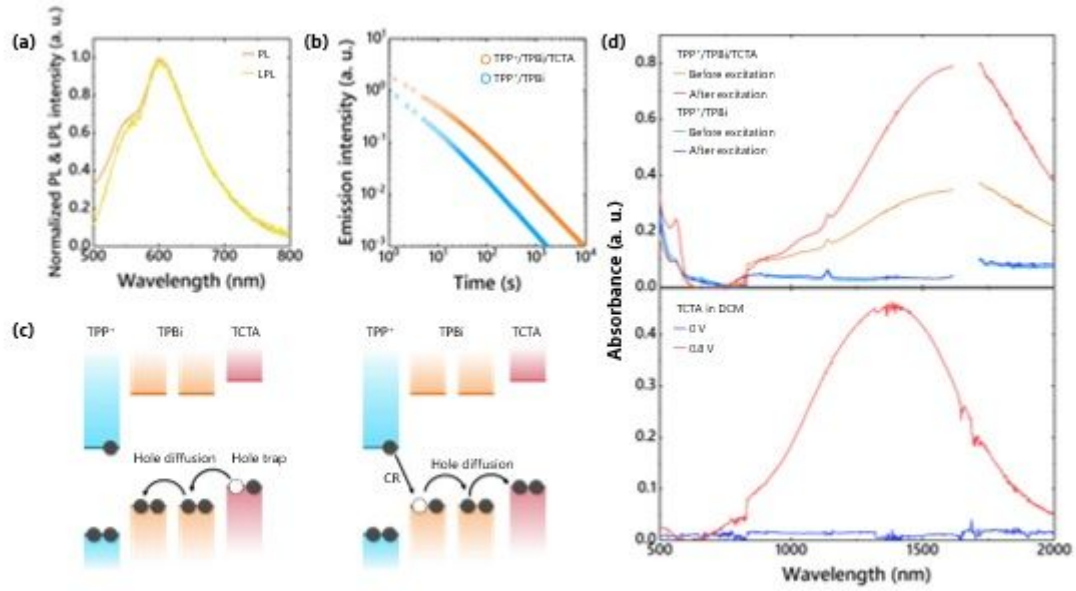

Figure 3

Photoluminescence properties of TPP+/TPBi/TCTA film under nitrogen gas. (a) PL and LPL spectra of TPP+/TPBi/TCTA film. (b) Emission decay profiles of TPP+/TPBi and TPP+/TPBi/TCTA films. (c) Emission mechanism of TPP+/TPBi/TCTA film. The TCTA molecule accepts holes from TPBi and forms radical cations because the HOMO level of the TCTA is shallower than that of the TPBi. Thermal detrapping from TCTA regenerates radical cations of TPBi and recombined with TPP radical. (d) (Top) Absorption spectra of TPP+/TPBi and TPP+/TPBi/TCTA films before and after photoexcitation. (Bottom) Absorption spectra of TCTA in DCM that contained 0.1 M TBAPF6 with and without electrical oxidation. Absorption data at 1600-nm omitted because of the quartz substrate absorption.

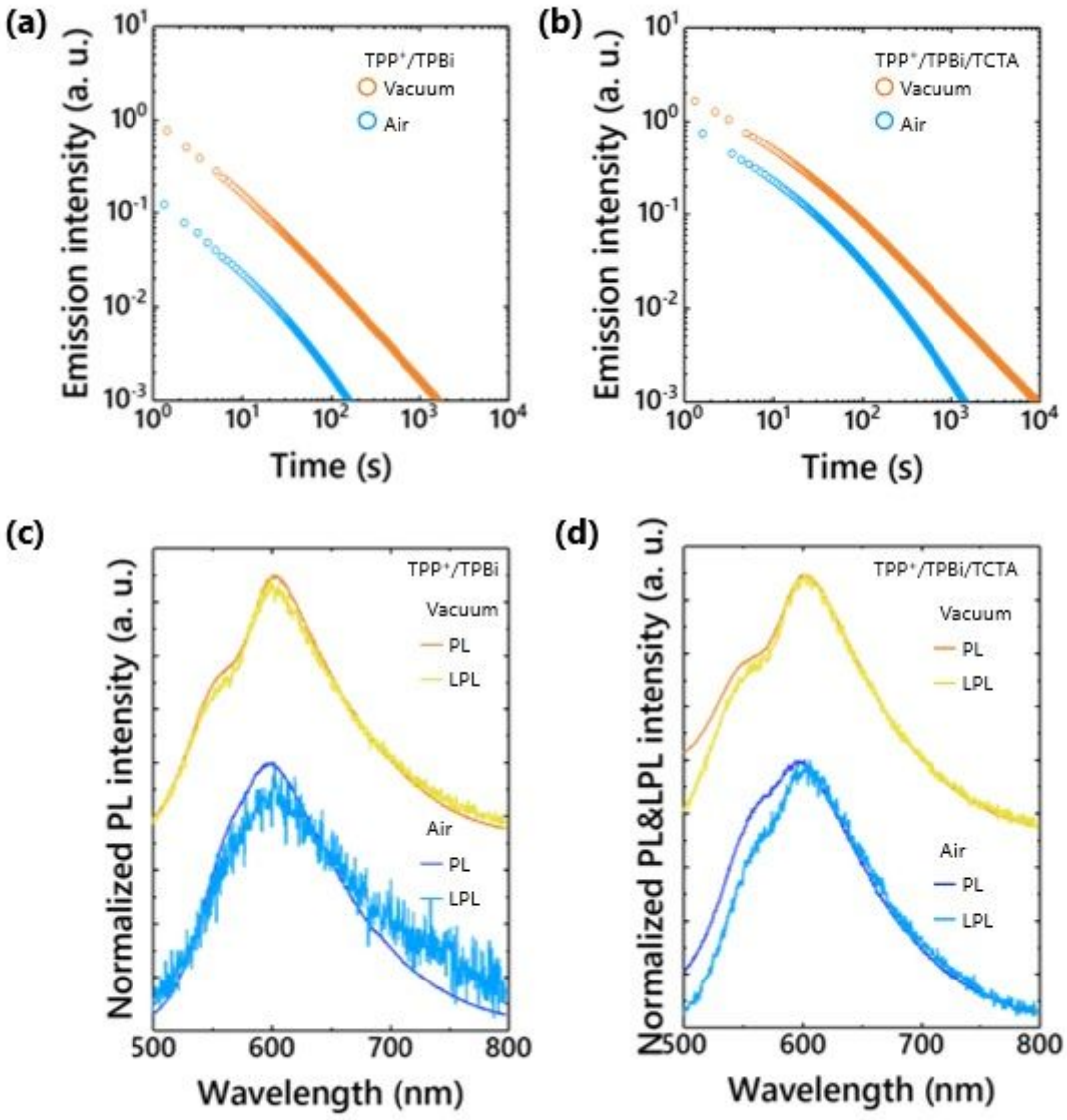

Figure 4

Optical properties of OLPL systems in air. LPL duration in vacuum and in air of TPP+/TPBi (a) and TPP+/TPBi/TCTA (b) films. PL and LPL spectra in vacuum and in air of TPP+/TPBi (c) and TPP+/TPBi/TCTA (d) films.

Supplementary Files

This is a list of supplementary files associated with this preprint. Click to download.

- VideoS1.mp4
- SupplementaryInformation.pdf